JOURNAL OF MATERIALS SCIENCE 30 (1995) 5885–5900

The failure of fibre composites and adhesively bonded fibre composites under high rates of test

Part I *Mode I loading–experimental studies*

B. R. K. BLACKMAN, J. P. DEAR, A. J. KINLOCH, H. MACGILLIVRAY, Y. WANG, J. G. WILLIAMS, P. YAYLA
Department of Mechanical Engineering, Imperial College of Science, Technology and Medicine, Exhibition Road, London SW7 2BX, UK

The failure of fibre composites and adhesively bonded fibre composites under high rates of test, up to rates of about 15 m s^{-1} were studied in detail. The present paper, Part I of the series, considers the experimental aspects of the mode I fracture of the fibre composite materials and joints. Part II will analyse the dynamic effects which are invariably associated with high-rate tests, and will show how these effects influence the observed behaviour of the test specimens. Part III will report the results from mode II and mixed-mode I/II tests on the fibre composite materials.

1. Introduction

One of the most important mechanical properties of a fibre composite, consisting of continuous fibres embedded in a polymeric matrix, is its resistance to delamination. The presence of delaminations may not only lead to complete fracture, but even partial delaminations will lead to a loss of stiffness which can be a very important design consideration. A popular approach to the characterization of the propagation of interlaminar cracks has been through the application of linear elastic fracture mechanics (LEFM) which enables the critical strain-energy release rate, or fracture energy, G_c, to be deduced [1–5]. Various modes of fracture may be identified. Mode I (tensile opening) is the lowest fracture energy for isotropic materials and, thus, a crack will always propagate along a path normal to the direction of maximum principal tensile stress. Hence, a crack in an isotropic plate will propagate in mode I fracture, regardless of the orientation of the initial flaw with respect to the applied stress. However, this is not necessarily the case for crack growth in fibre composites which are highly anisotropic materials. In these materials, the initial interlaminar defect is constrained and usually continues to propagate in the same plane between the laminate, regardless of the orientation of the crack to the applied loads. Thus, global mode II (in-plane shear) failures are possible and, obviously, mixed-mode I/II failures may also be observed. There has, therefore, been considerable interest in determining values of G_{Ic}, G_{IIc} and $G_{I/IIc}$.

One of the most widely used methods for joining fibre composites is via the use of structural adhesives [6]. This class of adhesives, typically based upon epoxy resins, possess a relatively high modulus and strength and are used to produce load-bearing joints. Again, LEFM has been widely used to study the failure resistance of bonded fibre-composite joints and many papers have been published [6] which consider the measurement and interpretation of the adhesive fracture energy, G_{Ic}, of such bonded joints.

As fibre-composites, and adhesively bonded fibre composite joints, have been increasingly used in demanding engineering applications, there has arisen an interest in the failure behaviour of such materials and bonded joints under high rates of test. However, relatively little work has been published in the literature, and the results which have been reported have been conflicting in nature. For example, Smiley and Pipes [7] reported a very large decrease in the value of G_{Ic} of both epoxy/unidirectional carbon-fibre and poly (ether–ether ketone) (PEEK) /unidirectional carbon-fibre composites as the rate of test was increased from 4.2×10^{-6} to 0.67 m s^{-1}. However, Beguelin *et al.* [8] have reported that the G_{Ic} of the PEEK/unidirectional carbon-fibre composite suffered only a small reduction as the rate of test was increased from about 1.7×10^{-5} to 1 m s^{-1}. Aliyu and Daniel [9] found that the value of G_{Ic} of an epoxy/unidirectional carbon-fibre composite actually increased slightly as the test rate was increased. Although, Yaniv and Daniel [10] subsequently reported that this initial increase was followed by a decrease in G_{Ic} as the test rate was further increased. In the case of mode II failure, a modest decrease in toughness with increasing rate of test has been reported by Maikuma *et al.* [11].

The present work aimed to study in detail the failure of fibre composites and adhesively bonded fibre composites under high rates of test. The present paper, Part I of the series, considers the experimental aspects of the mode I fracture of the fibre composite materials

0022–2461

and joints. Part II [12] will analyse the dynamic effects which are invariably associated with high-rate tests, and will show how these effects influence the observed behaviour of the test specimens. Indeed, the experimental difficulties of conducting high-rate tests and the strong dynamic effects which are frequently present, are important factors in explaining the conflicting findings reported in the literature. Part III [13] will report the results from mode II and mixed-mode I/II tests on the fibre composite materials.

2. Theoretical considerations

In the standard mode I double-cantilever beam (DCB) test, the crack is centrally located, as shown in Fig. 1, and the two arms of the specimen are subjected to equal and opposite bending moments. The value of the interlaminar fracture energy, G_{Ic}, may be expressed [3] by

$$G_{Ic} = \frac{12P_c^2a^2}{B^2h^3E_{11}} \tag{1}$$

where B is the width and $2h$ is the combined thickness of fibre composite arms, a is the crack length, P_c is the critical load required to induce crack growth and E_{11} is the axial modulus of the fibre composite arms.

However, the above equation needs to be corrected [3] for various effects which are not accounted for in the simple beam theory used above. Such effects arise due to (i) large deflections of the arm, (ii) stiffening of the arms due to the presence of the end blocks, and (iii) shear deformation and deflection at the crack tip. The large deflection and end-block effects may be taken into account by using the correction factors F and N. The values of F and N may be found from the expressions previously given [3]

$$F = 1 - \theta_1(\delta/L)^2 - \theta_2(\delta l_1/L)^2 \tag{2}$$

where l_1 is the distance of the load-point above the beam axis, L is the length of the arms of the specimen (i.e. $L = a$) and δ is the displacement of the arms of the DCB specimen, and

$$N = 1 - \theta_3(l_2/L)^3 - \theta_4(\delta l_1/L^2) - \theta_5(\delta/L)^2 \tag{3}$$

where l_2 is the half-width of the end-block. For the mode I DCB specimen, the values of the constants are

$$\theta_1 = 3/10, \theta_2 = 3/2, \theta_3 = 1,$$
$$\theta_4 = \frac{9}{8}[1 - (l_2/a)^2], \theta_5 = \frac{9}{35} \tag{4}$$

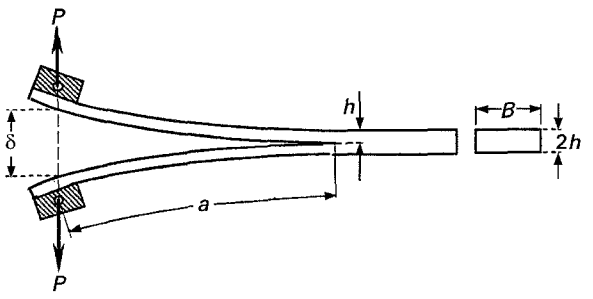

Figure 1 The double cantilever beam (DCB) composite specimen.

The correction factor, χ_I may be introduced [3] for end-rotation and deflection of the crack tip. The value of χ_I may be ascertained from the expression for the corrected compliance, C, where

$$C = \frac{\delta}{P} = \frac{8N(a + \chi_I h)^3}{Bh^3E_{11}} \tag{5}$$

Now, from Equation 5, the value of χ_I may be deduced by plotting $(C/N)^{1/3}$ versus the corresponding value of the crack length, a, and the intercept yields the value of the correction factor χ_I. Also, from the slope of the linear relationship, the value of E_{11} may be determined. A typical plot of $(C/N)^{1/3}$ versus the corresponding value of the crack length, a, is shown in Fig. 2, and an excellent linear relationship is obtained. The average value of χ_I, deduced for the PEEK/carbon-fibre composite, was 2.4 and for the epoxy/carbon-fibre composite was 3.0. In the case of the adhesively bonded fibre composite joints the average value of χ_I was 3.8.

The expression for the modulus, E_{11}, which may be determined from the DCB test, is now given by

$$E_{11} = \frac{P}{\delta}\frac{8N(a + \chi_I h)^3}{Bh^3} \tag{6}$$

The corrected value of the mode I interlaminar fracture energy, G_{Ic}, may be deduced from either the "corrected-load" method

$$G_{Ic} = \frac{12FP_c^2(a + \chi_I h)^2}{B^2h^3E_{11}} \tag{7}$$

or the "corrected-displacement" method

$$G_{Ic} = \frac{3}{2}\frac{F}{N}\frac{P_c\delta_c}{B(a + \chi_I h)} \tag{8}$$

where δ_c is the critical displacement.

However, as will be shown later, a problem that arises with the high-rate tests is that the measured load oscillates violently and an accurate load, P_c, cannot be measured, although the displacement, δ_c, and corresponding crack length, a, can be determined from high-speed photography. Hence, we may combine Equations 6 and 8 to obtain an expression for G_{Ic} which does not require a direct knowledge of the load, namely

$$G_{Ic} = \frac{3}{16}\frac{F}{N^2}\frac{\delta_c^2h^3E_{11}}{(a + \chi_I h)^4} \tag{9}$$

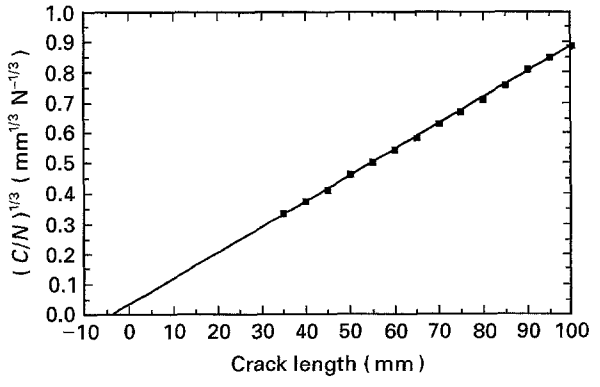

Figure 2 $(C/N)^{1/3}$ versus the crack length, a.

This form of expression for obtaining values of G_{Ic} was employed for all test rates and the value of the modulus, E_{11} used was determined from three-point bend tests and ultrasonic tests, as described below.

3. Experimental procedure

3.1. Materials

3.1.1 Fibre composite specimens

Two different polymeric fibre composites were used in the present studies:

(i) a unidirectional carbon-fibre poly (ether–ether) ketone (PEEK) composite (APC-2, supplied by ICI plc, UK). The volume fraction of the thermoplastic PEEK matrix was nominally 35% and the carbon fibres were AS4 type (from Hercules Inc., USA);

(ii) a unidirectional carbon-fibre epoxy-resin composite (Fibredux 6376C supplied by Ciba Composites, UK). The volume fraction of the thermosetting matrix was nominally 35% and the carbon fibres were T-400 type (from Toray Inc., Japan).

Unidirectional laminate sheets of APC-2 were moulded using a hot press, according to the manufacturer's instructions. The epoxy/carbon-fibre composite was cured in an autoclave, according to the manufacturer's instructions.

3.1.2. Adhesively bonded fibre composite specimens

The polymeric fibre composite which was used as the substrate for the adhesively bonded specimens was an epoxy/unidirectional carbon fibre (913C XAS-5-34% composite from Ciba Composites, UK), a thermoset composite with a modified epoxy-resin matrix. It was a continuous carbon-fibre composite containing a volume fraction of fibres of about 63%. Curing was conducted using a hot press, according to the manufacturer's instructions.

3.2. Preparation of specimens

3.2.1. Fibre composite specimens

The fibre composite specimens were prepared in the form of DCB specimens as shown in Fig. 1. The initial delamination was made by moulding in a double layer of aluminium foil having a total thickness of 20 μm and a length of 25 mm. This double-layer insert was, however, stepped, such that the part of the insert closest to the crack tip was effectively a single layer. This resulted in a relatively low insert thickness of 12 μm which formed the initial delamination, from which crack growth occurred. Aluminium end-blocks were then bonded on to each side at the end of the specimen where the initial delamination was present and the edge of the specimen was painted with a white typewriter correction liquid and marked at 5 mm intervals to enable the crack length to be monitored during the test.

Prior to the actual failure tests, the initial delamination in the fibre composite specimens created by the presence of the aluminium foil insert, was extended to a length, a_p, of 35 mm under mode II loading, i.e. the foil crack was grown by conducting [3] a mode II test at a constant displacement rate of 0.5 mm min^{-1}. (Mode II loading was used to avoid the development of any fibre bridging which might have occurred [14] under mode I loading.)

3.2.2. Adhesively bonded fibre composite specimens

The adhesive joints were prepared in the form of DCB specimens as shown in Fig. 3. The substrates were cut from the laminate sheet, of thickness 1.5 mm, and were 20 mm wide. The adhesive employed was either a two-part cold-cured epoxy-paste adhesive (EA 9309 from Hysol Dexter, USA) or a one-part hot-cured epoxy-film adhesive (FM73M, from American Cyanamid, USA). The bondline thickness was controlled when using the film adhesive by a polyester mat carrier incorporated into the film. Four layers of the epoxy film provided a uniform bondline thickness of 0.35 mm. When using the epoxy-paste adhesive, the bondline thickness was controlled by the addition of 0.5% by mass of 0.35 mm glass beads to the adhesive.

The initial starter crack was made by inserting a double layer of release-coated aluminium foil. Again the foil was stepped at the end to provide an initial delamination thickness of 12 μm in between the adhesive-coated composite substrates. To effect cure of the adhesive, the joints prepared using the two-part cold-cured epoxy-paste adhesive were held at 21 ± 2 °C under a pressure of 69 kPa for 4 days, whilst those using the one-part hot cured epoxy-film adhesive were held at 120 °C for 1 h under a pressure of 275 kPa. The test specimen was completed by bonding on to each side of the DCB joint the aluminium end-blocks, using a room-temperature curing toughened adhesive. The edges of the DCB specimens were painted white using a typewriter correction fluid and were marked off at 5 mm intervals along the complete length of the beam. The adhesive joint specimens were not precracked, because no "resin-rich" zone could develop ahead of the crack, as it might for the fibre composite materials. Indeed no problems with initial crack blunting, or the subsequent development of an R-curve, were observed with the adhesive materials. Thus, the crack was allowed to initiate directly from the aluminium-foil insert during the test.

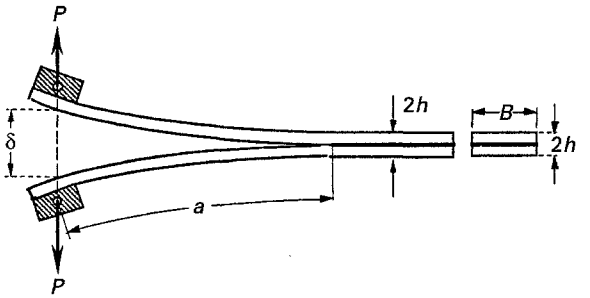

Figure 3 The double cantilever beam (DCB) adhesive joint specimen.

3.3. Fracture test methods

3.3.1. Slow-rate tests

Slow-rate tests were performed using a screw-driven tensile-testing machine. The test temperature was $22 \pm 1\,^{\circ}C$. The tests were conducted in displacement control at a rate of $2\,mm\,min^{-1}$. The load and displacement were recorded using the chart recorder, and the length of the growing crack was monitored by the use of a travelling microscope mounted in front of the specimen. Each time the crack front passed a 5 mm marker on the side of the specimen, the chart was marked, so that the corresponding values of P and δ could be recorded.

3.3.2. High-rate tests

Tests at intermediate rates, i.e. up to $1.67 \times 10^{-2}\,m\,s^{-1}$, were conducted using the screw-driven tensile testing machine as described previously. However, at all but the slowest rates it was, of course, not possible to monitor the crack propagation visually. Therefore, at all rates faster than $1.67 \times 10^{-4}\,m\,s^{-1}$, high-speed photography was used to record the displacement, δ, and crack length, a. At test rates in excess of $1.67 \times 10^{-2}\,m\,s^{-1}$ and up to $15\,m\,s^{-1}$, a servo-hydraulic testing machine, with associated high-speed data acquisition facilities, was used. The tests were conducted at a temperature of $23 \pm 2\,^{\circ}C$.

The high-rate test rig is shown schematically in Fig. 4. The servo-hydraulic testing machine (an Instron Model 1343) was capable of displacement rates of up to $25\,m\,s^{-1}$ and was equipped with a piezoelectric load cell with a signal amplifier. The data were acquired using a 20 MHz digital oscilloscope (Gould 1600 series) and a 486 Personal Computer loaded with Dadisp signal analysis software. Each test was photographed using a high-speed camera. This was a Hadland 16 mm Photec (IV) camera, with a maximum operating speed of 40,000 frames per second. The optics incorporated a 45 mm, f 2.8 lens, a rotating prism and an associated half-frame image converter. A 16 mm tungsten-balanced 7250 Eastman Film was used to provide a high-resolution, colour record of the test. To achieve the correct exposure levels, a variable-focus tungsten spotlight was employed. This was activated immediately prior to the test to avoid any significant heating of the specimen. Incorporated into the camera was a timing-light generator which marked the film with a 100 Hz time base for a camera speed of less than 2000 frames per second, and with a 1 kHz time base for a camera speed of greater than 2000 frames per second. To determine the actual specimen displacement, δ, and the crack length, a, at any time during the test the film negative was projected, and so greatly enlarged, on to a screen, from which accurate measurements could be made. A projector was used which could project individual frames from the high-speed film.

Details of the loading arrangement for the high-rate mode I DCB test are shown in Fig. 5. The DCB specimens were fixed on to the test rig between two specially designed titanium shackles. The upper shackle was fixed to a titanium "lost motion device" (LMD) which was inserted directly into the hydraulic ram of the test machine. We will return to the function of the LMD below. The lower shackle, on the stationary side of the specimen, was coupled to the piezoelectric load cell. The load cell was selected for its high natural frequency of 70 kHz and its short rise-time of 10 μs. Its output signal was amplified and then passed to the oscilloscope. For reference, the oscilloscope also captured the signal from the displacement transducer mounted on the ram. Thus, a record of the load versus time and the ram displacement versus time signals were captured on the oscilloscope for each test. Prior to conducting the tests, the position of the LMD was set to allow a period of pre-travel to ensure that the test was conducted at constant velocity. Tests were then performed at rates from 1×10^{-2} to $15\,m\,s^{-1}$. The oscilloscope and camera were triggered in order

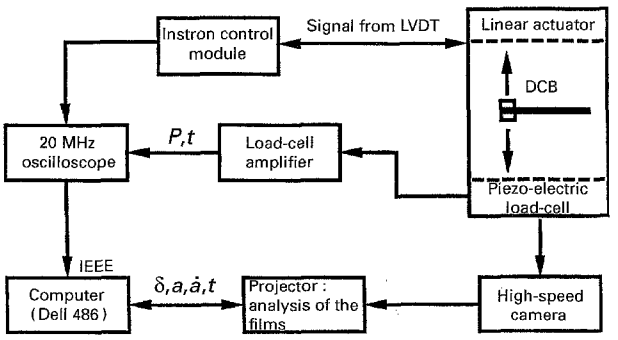

Figure 4 A schematic diagram of the high-rate test rig.

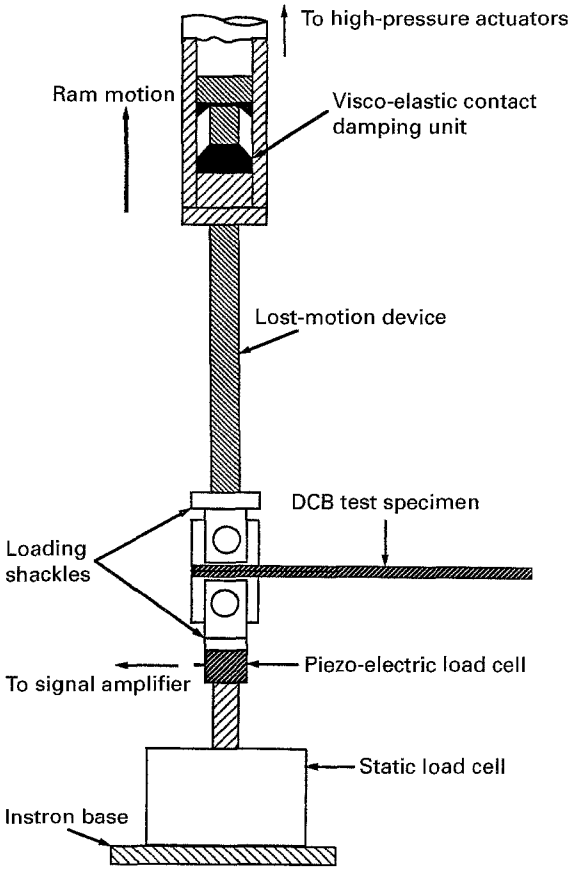

Figure 5 The loading arrangement for the DCB tests.

to capture the values of the load, ram displacement, specimen displacement and crack length as a function of time. Timing marks on the high-speed film record provided an accurate time base, such that the specimen displacement and crack length values could be accurately correlated to the measured values of the load. The signals were transferred to the dedicated computer, where they could be analysed using the signal analysis software.

Returning to the design and function of the "lost motion device" (LMD), the purpose of this device was to ensure that the ram had attained a constant velocity before motion was transferred to the specimen. The nature of the contact area between the LMD and the hydraulic ram was found to have a considerable bearing on the dynamics of the test. If the contact surfaces between the LMD and the hydraulic ram had been left unmodified then, on contact, the initial velocity of the LMD (and hence the specimen) would have been greater than that of the ram. Thus, a bouncing effect would have occurred between the LMD and the ram, resulting in a test with a transient loading rate. This phenomenon has also been reported by other workers [8, 15], who therefore modified the contact stiffness by the insertion of a viscoelastic material. If such a modification is made, the impact is damped and the specimen may be smoothly accelerated. Clearly, as an increasing amount of viscoelastic material is inserted between the contact surfaces, the more gradually the specimen accelerates, and thus the slower the effective test rate. In the present work, rubber was inserted between an "aluminium cup and cone" contact area. This particular design was chosen because the inclined contact area resulted in a smoother take-up of the LMD and provided a larger potential damping area. Finally, it should be noted that the extent of the loss of contact may be varied by employing different, and different amounts of, the viscoelastic damping material.

From the above observations it is important to note that the displacement of the specimen should *not* be deduced from the output of the displacement transducer monitoring the position of the hydraulic ram of the test machine, because this can lead to very misleading results being obtained. In the present work, all displacement values used in the various equations were obtained using high-speed photography to record the actual deformations of the arms of the specimen during the test. The values of displacement so determined were not, therefore, subject to errors caused by any dynamic acceleration and oscillation effects, and/or loss of contact of the LMD during loading. To illustrate these aspects, the high-speed film was used to determine accurately the actual specimen displacement at any instant during the test, and such values were compared to the values of the displacement of the ram of the test machine, measured using the transducer connected to the ram. It may be seen from Fig. 6a that, at a test rate of 1 m s^{-1}, the displacement of the ram quite accurately predicts the displacement of the specimen. However, Fig. 6b shows that at a test rate of 15 m s^{-1}, the displacement of the ram cannot be used to predict the displacement of the

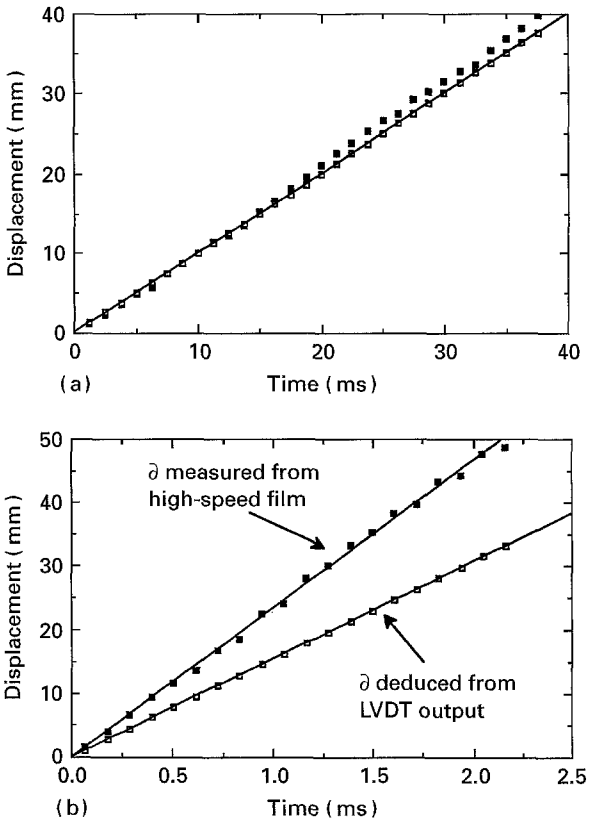

Figure 6 (□) Ram displacement and (■) actual specimen displacement versus time from tests conducted using an adhesively bonded DCB specimen at a ram-displacement rate of (a) 1 m s^{-1}, (b) 15 m s^{-1}.

specimen. Thus, if the specimen displacement was deduced from the ram displacement, the result would be to underestimate significantly the actual displacement as correctly recorded from high-speed film, and thus underestimate significantly the resulting value of G_{Ic} as determined from Equation 9. This significantly greater velocity of the specimen, compared to the ram of the test machine, is yet another aspect of the complex dynamic effects [12] observed in high-speed experiments.

3.4. Evaluation of the axial modulus, E_{11}, of the fibre composites

3.4.1. Flexural tests

To obtain accurate values for the axial modulus of the fibre composites tested, a number of three-point bend tests was undertaken. Using composite beams, possessing an identical geometry and lay-up to those used in the fracture tests, a series of three-point bend tests was conducted at a constant displacement rate of 0.5 mm min^{-1}. In order to ensure high accuracy, an external transducer was used to measure the displacement of the beam during the test. It was noted that very good agreement was obtained between the values of the modulus calculated from beam theory following a mode I fracture test and the values measured using the three-point bend test. The values obtained were 120 GPa for the epoxy/carbon-fibre composite and 115 GPa for the PEEK/carbon-fibre composite.

3.4.2. Ultrasonic measurements

The moduli of the fibre composites were also measured using an ultrasonic technique. Ultrasonic tests were conducted in order to investigate whether the moduli of any of the fibre composites were significantly dependent upon the strain rate. Clearly, when undertaking fracture tests at rates of up to 15 m s^{-1}, it is important to use the correct values of E_{11} in the beam theory equations when calculating values of G_c.

Various ultrasonic test methods are available, and the method followed in the present work utilized the propagation of Lamb waves [16] in thin plates of the fibre composite material. Lamb waves are two-dimensional vibrational modes which propagate in free plates. There are a number of different modes of Lamb wave, e.g. flexural, termed α_0, and longitudinal, termed s_0. When these "zero order" Lamb waves combine they form what is effectively a Rayleigh wave. In the present work, the longitudinal, (s_0), wave has been utilized. It was shown by Kolsky [17] that, as the frequency times thickness product tends to zero, the phase velocity of s_0 tends to the velocity of the longitudinal plate wave, c_0, which is given by

$$c_0 = \left[\frac{E_{11}}{\rho(1-\upsilon^2)}\right]^{1/2} \quad (10)$$

for plane-strain conditions in the plate, where ρ is the density and v is the Poisson's ratio of the material. Thus, if the s_0 longitudinal vibrational mode can be propagated without the introduction of other modes and without significant dispersion, then the longitudinal modulus E_{11} can be deduced for the plate, as a function of frequency.

The experimental test rig employed is shown in Fig. 7. Essentially, a pulse and function generator were used to produce a tone burst of excitation at a particular frequency, which was amplified and passed to the transducer at the transmitter station. The transducer was coupled to the plate by the use of an angled poly(methyl methacrylate) wedge. An optimum angle for this wedge existed when the amplitude of the s_0 vibrational mode relative to other modes in the plate was a maximum. For the fibre composite materials under investigation, this angle was found to be 20°. A thin film of water was used to couple the wedge to the plate.

The vibrational pulse propagated primarily in the longitudinal direction of the plate in the direction of the transducer at the receiver station. This transducer was also coupled to the plate at the same angle of inclination. This received signal was amplified and captured on the oscilloscope. The twice-reflected signal is also detected by this transducer and captured on oscilloscope. This total signal was then transferred to a computer. A spectrum analyser with a two-dimensional fast-Fourier transform facility was then utilized to ensure that significant dispersion of the wave had not occurred. Next, by measuring the time elapsed between the captured signals, the velocity of the longitudinal, s_0, wave was determined. The frequency of the tone burst could be altered by using a computer program, and frequencies from 240 kHz to 1.06 MHz were employed. This frequency range represented the effective limits of applicability of this technique when using specimens which could be readily manufactured.

The parameters used in the calculation of E_{11} from Equation 10 are given in Table I. The density of the fibre composites was measured and is given by ρ. The Poisson's ratio is given by v which was obtained from the manufacturers' data, the term L_p is the length of the plate employed, and is required for the wave-speed measurements.

The results in Table II show that for the epoxy composite the values of E_{11} vary from 119–113 GPa. These values are in very close agreement with the values obtained from the three-point bend tests, and from the DCB tests using corrected beam theory, both of which were conducted at relatively slow rates of test. Similarly, the results in Table III show that for the PEEK composite, the values of E_{11} vary from 115–112 GPa for the ultrasonic technique. Again, these values are in very close agreement with the values obtained at slow rates of test. These results are in agreement with results published by Harding and Welsh [18], which also indicated that the axial moduli of these unidirectional carbon-fibre composites are not significantly strain-rate dependent. Thus, the static, low-rate, value of E_{11} may be used in Equation 9.

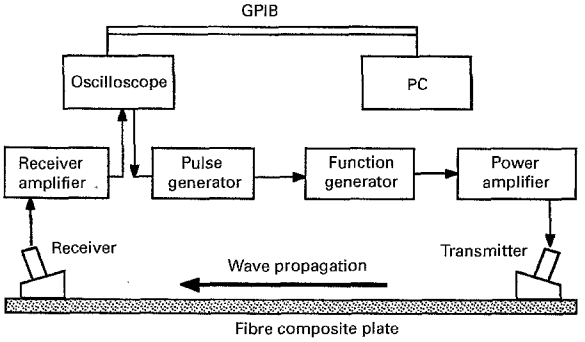

Figure 7 A schematic diagram of the ultrasonic test rig.

TABLE I Parameters used to deduce the value of E_{11}

Parameter	Epoxy composite	PEEK composite
ρ (kg m^{-3})	1566	1540
v	0.27	0.28
L_p(mm)	291	286

TABLE II Results for the epoxy composite

Frequency (kHz)	Time (μs)	Wave speed (m s^{-1})	E_{11} (GPa)
240	64.3	9051	118.9
400	64.5	9023	118.2
600	64.5	9023	118.2
800	64.6	9009	117.8
900	64.8	8981	117.1
1000	65.4	8899	115.0
1050	65.8	8845	113.6
1060	65.9	8832	113.2

TABLE III Results for the PEEK composite

Frequency (kHz)	Time (μs)	Wave speed ($m s^{-1}$)	E_{11} (GPa)
240	63.5	9008	115.2
450	63.6	8994	114.8
600	63.7	8980	114.4
650	64.1	8924	113.0
870	63.9	8951	113.7
940	64.0	8938	113.7
980	64.1	8924	113.0
1030	64.5	8868	111.6

4. Results and discussion: fibre composite specimens

4.1. Load versus time traces

The load versus time traces for the PEEK/unidirectional carbon–fibre composites tested at four different rates of test are shown in Fig. 8. Several interesting points emerge from these data.

Firstly, at a rate of test of 3.3×10^{-5} m s^{-1} the load versus time trace (Fig. 8a) is associated with the crack growing in a stable, continuous manner through the DCB specimen. However, at rates greater than about 8.3×10^{-5} m s^{-1} there is a clear tendency for unstable, "stick-slip", crack growth to be observed. This may be seen from Fig. 8b which shows the load versus time trace for this material at a test rate of 1×10^{-2} m s^{-1}. In this figure the deviation from linearity of the initial slope of load versus time trace is associated with stable crack growth, but this short period of stable cracking is followed by rapid crack growth which leads to crack arrest. This sequence of a short period of stable crack growth followed by unstable crack growth is then repeated down the length of the DCB specimen. This sequence can also be clearly seen for a test rate of 0.5 m s^{-1} (Fig. 8c).

However, secondly, Fig. 8c and d show another major effect of increasing the test rate. Namely, the presence of an increasing number of oscillations on the trace which arise from dynamic effects. As was discussed earlier, the load versus time signals were never filtered, because it is not possible to know which part of the signal represents the true behaviour of the specimen and which parts reflect the purely dynamic effects. These dynamic effects are likely to arise from several causes. The first peak in the load versus time trace is very likely to be greatly influenced by inertial effects. On the other hand, the following multiple oscillations are likely to be caused by stress waves propagating in the specimen. For example, the DCB specimen may respond and deform due to the propagation of shear waves through the specimen. The shear-wave speed is in the order of 5000 m s^{-1}, and these waves therefore propagate with a frequency in the range of 30–50 kHz. Flexural waves also occur in the DCB specimen and their wave speed is a function of crack length. The typical flexural wave speed is in the range of 200–1000 m s^{-1}, and therefore propagates with a frequency below about 1 kHz. Indeed, if the higher frequency oscillations are filtered out, then these lower frequency flexural wave effects can be readily observed. Another possible cause of the multiple oscillations is that the shear waves, having a frequency of about 30–50 kHz, are of the appropriate frequency to create resonant effects in the piezo-electric load cell. Recall that the load cell has a natural

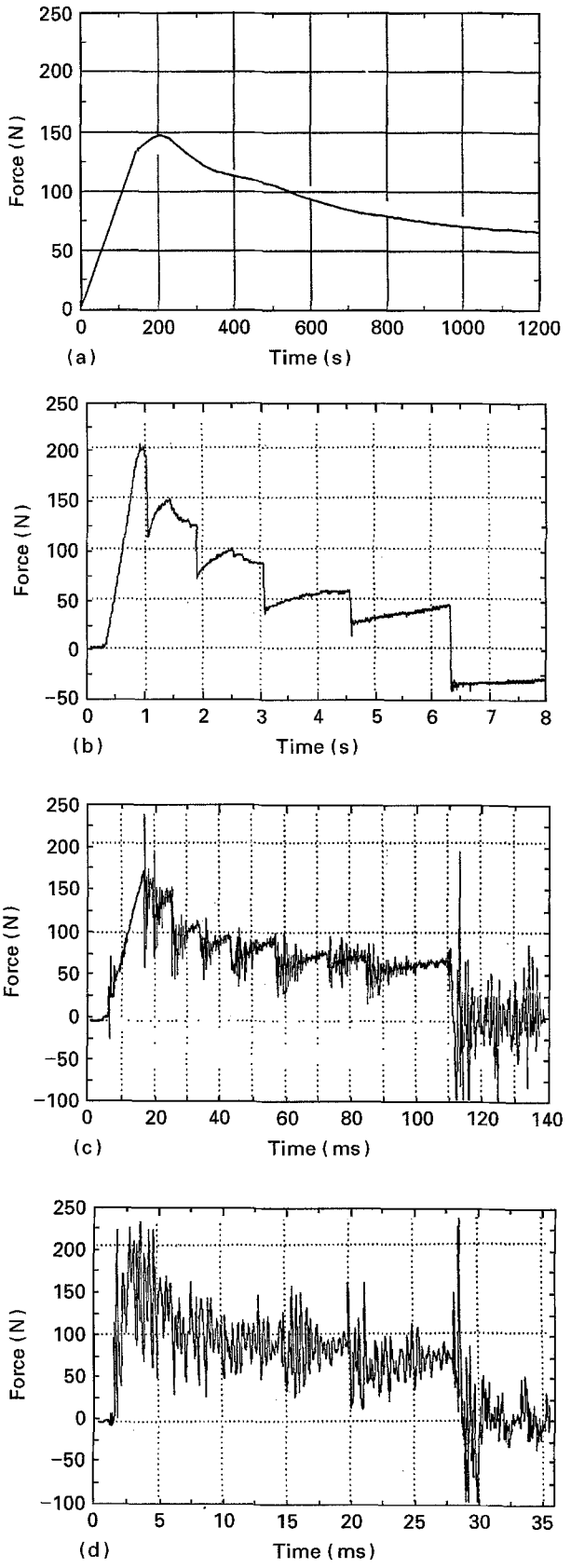

Figure 8 Typical load versus time traces for PEEK/carbon-fibre composite tests conducted at a ram-displacement rate of (a) 3.3×10^{-5} m s^{-1}, (b) 1×10^{-2} m s^{-1}, (c) 5×10^{-1} m s^{-1}, (d) 2 m s^{-1}.

frequency of about 70 kHz, but this is lowered somewhat when the loading shackles are connected to the cell. Finally, it should be noted that the longitudinal wave speed is about 9000 $m\,s^{-1}$, and this is considered to be too high to affect the load traces significantly.

Thirdly, the above effects lead to the problem that, whilst the load versus time traces obtained at the lower rates of 3.3×10^{-5} and 1×10^{-2} $m\,s^{-1}$, can be readily interpreted and analysed to yield values of the interlaminar fracture energy, G_{Ic}, the traces from the higher rates of test cannot be readily interpreted. Also, any load values obtained from such traces are very susceptible to errors, because the true load representing the material behaviour may be completely obscured by the dynamic effects. It is for these reasons that Equation 9 was derived, which enables the values of the fracture energy to be obtained without requiring a knowledge of the load applied to the specimen. However, it should be noted that Equation 9 is a "static" analysis. It does not take into account dynamic effects due either to kinetic energy contributions or to stress waves propagating in the specimen. These effects are considered in Part II [12].

Turning to the epoxy/unidirectional carbon-fibre composite, for this material the crack propagated in a relatively stable, continuous manner over the complete range of test rates, with the load versus time traces revealing no obvious indication of a transition from stable to typical unstable ("stick–slip") crack growth as observed for the PEEK composite. Thus, clearly the transition from stable crack growth to unstable crack growth is not only a function of the test specimen geometry and loading conditions, but also of the actual material under study. However, as observed for the PEEK/unidirectional carbon-fibre composites, the load versus time traces became more complex in nature as the rate of test was increased, with an

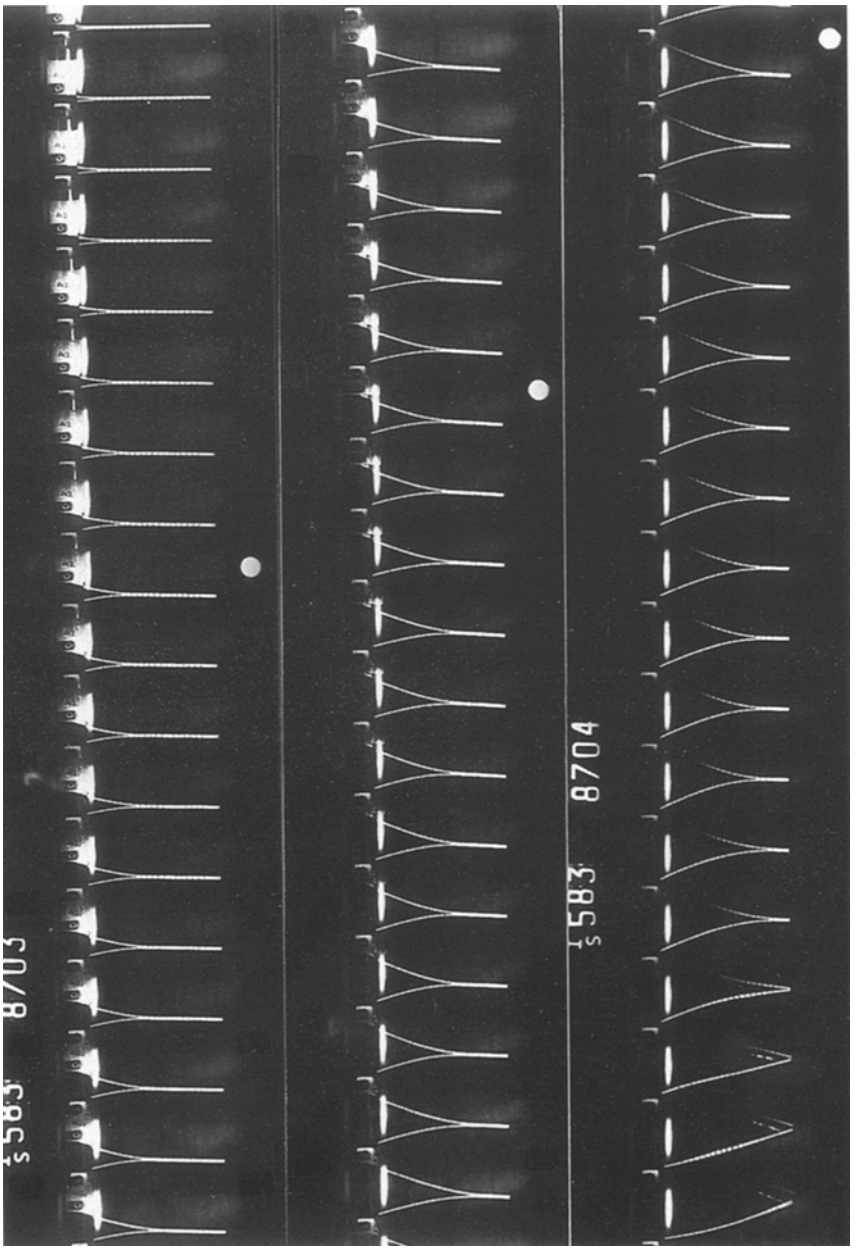

Figure 9 A high-speed film sequence showing the photographic record of a mode I interlaminar DCB test conducted at a ram-displacement rate of 2 $m\,s^{-1}$. The material was PEEK/carbon-fibre composite. The framing rate was 1500 frames per second and the sequence is from top to bottom of strip one, then two and then three.

increasing number of oscillations being recorded due to dynamic effects at the higher test rates.

4.2. Variation of crack length and crack velocity with time

In the case of the relatively slow rate tests, the variation of the crack length with time during the test could be monitored by visual observation, with the aid of a travelling microscope. For the higher rate tests, the relationship between crack length and rate was obtained via analysis of the high-speed film which recorded the progress of the test. A typical sequence of the high-speed film is shown in Fig. 9, and this example is for a PEEK/carbon-fibre composite tested at a rate of $2\,m\,s^{-1}$. The circular white marks which may be seen to the right of the frames are timing marks, and are placed on to the film at 10 ms intervals. They show that the framing rate employed for this test was 1500 frames per second and allow the exact time interval between successive frames to be calculated. The high-speed film sequence shows clearly the position of the crack tip throughout the test and in this example it enabled the crack length, a, and beam opening displacement, δ, to be measured at time intervals of 0.66 ms during the test. This test lasted 33 ms.

Fig. 10a shows the variation of the length of the propagating crack with time for the PEEK/carbon-fibre composite tested at a rate of $3.3 \times 10^{-5}\,m\,s^{-1}$ (The onset of crack propagation is shown in each of the crack length versus time plots for reference.) As may be seen, the crack grows steadily during the test and the resulting crack velocity through the DCB specimen is shown in Fig. 10b. At the constant test rate of $3.3 \times 10^{-5}\,m\,s^{-1}$, the initial crack velocity is about $8 \times 10^{-5}\,m\,s^{-1}$ and steadily decreases to about $5 \times 10^{-5}\,m\,s^{-1}$. Fig. 10c and d show the variation of

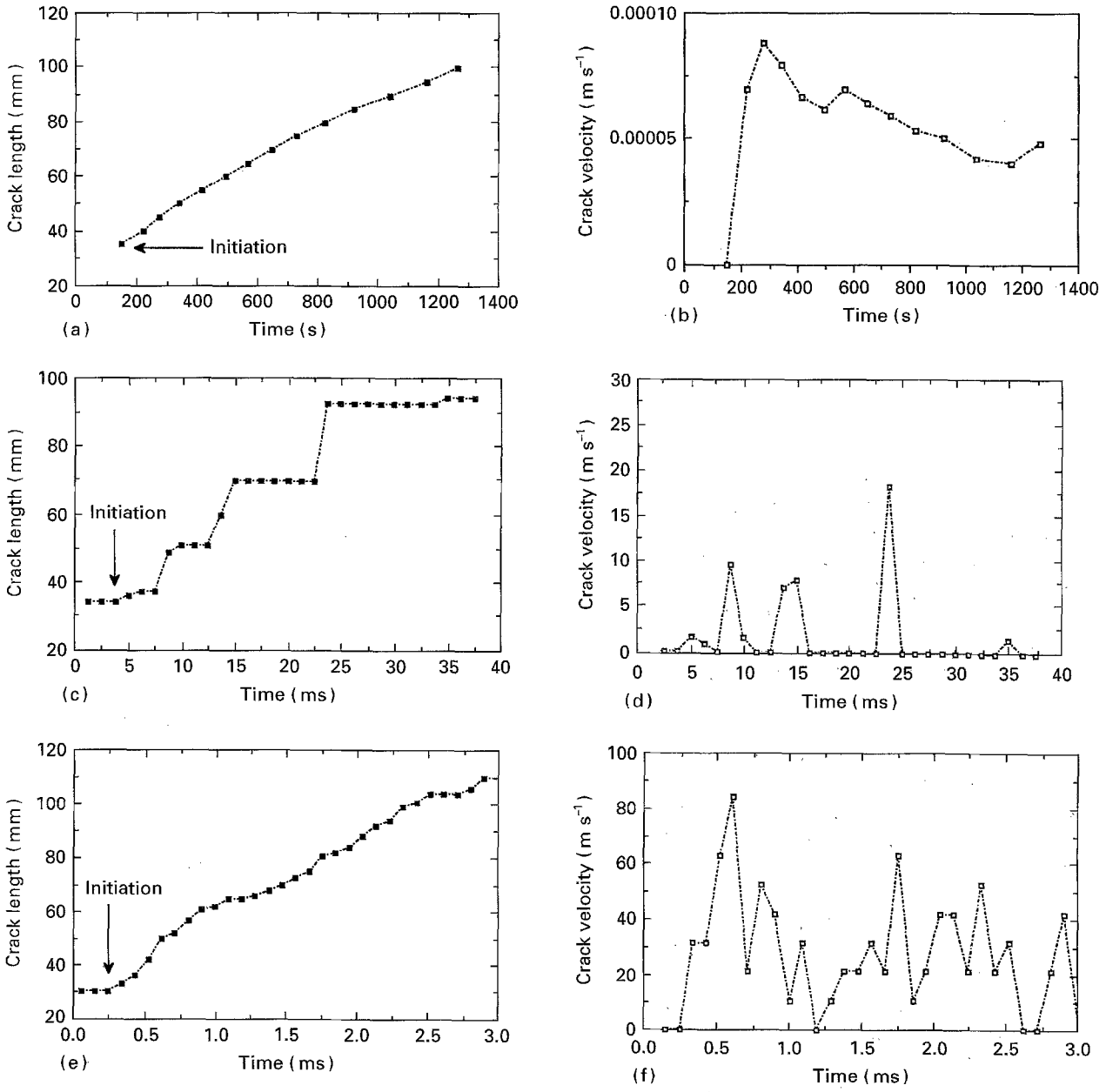

Figure 10 Typical (a, c, e) crack length and (b, d, f) crack velocity versus time traces for PEEK/carbon-fibre composite tests conducted at a ram-displacement rate of (a, b) $3.3 \times 10^{-5}\,m\,s^{-1}$, (c, d) $1\,m\,s^{-1}$ (e, f) $10\,m\,s^{-1}$.

the length of the propagating crack with time at a test rate of 1 m s^{-1}. This figure clearly illustrates the unstable, "stick-slip" crack growth which occurs in the PEEK composite at this test rate. The variation of crack velocity with time, Figure 10d, again reflects this type of crack growth. Here the crack propagates in spurts, with the crack velocity being of the order of several metres per second before crack arrest occurs, when the velocity is, of course, zero. The results obtained from a test at 10 m s^{-1} are given in Fig. 10e, f. At this test rate the crack propagation was again "stick–slip", but the crack length distance between the "stick–slip" regions was shorter, giving the appearance of more stable crack growth. However, an examination of the fracture surfaces clearly revealed that the crack growth was still of the "stick–slip" type. Indeed, Fig. 10f shows the highly transient nature of the crack velocity versus time relationship, with maximum crack velocities now significantly higher (up to about 80 m s^{-1}) in comparison to the values measured for the slower test rates, as would be expected for this very high test rate.

From the previous comments on the load versus time traces for the epoxy/unidirectional carbon-fibre composite it would be expected that the crack length versus time, and crack velocity versus time, traces would show steady, stable crack growth. This was indeed observed at the lower rates of test. However, at the relatively high rates of test a more unstable type of crack growth was observed, as was previously seen for the PEEK composite. Fig. 11a, for the epoxy composite, shows the length of the propagating crack plotted against time for a test conducted at 5 m s^{-1}, and the resulting crack velocity is shown in Fig. 11b. Note that irregular acceleration and deceleration of the crack does occur, and this probably arises from dynamic effects. The maximum crack velocity attained is about 90 m s^{-1}, and this is very quickly followed by a period of crack arrest when the velocity is zero. Fig. 11c and d show that similar transient behaviour occurs for a test conducted at 15 m s^{-1}, and clearly this test is even more affected by dynamic oscillations. Thus, although not readily evident from the load versus time traces, the higher test rates do give rise to irregular crack growth in the epoxy composite, with transients being observed in the crack speed as it propagates through the DCB specimen.

At the higher rates, precisely defining the instant of crack initiation was achieved using high-speed photography. Thus, the accuracy of the instant of crack initiation was simply limited by the fact that the observation of the specimen is not continuous, but occurs at discrete points represented by the interval between frames, which depends upon the camera speed. However, with the high framing rates possible with the high-speed camera which we used, a high degree of accuracy could be attained for the measured values of crack length, a, and displacement, δ, for crack initiation. Hence, Equation 9 could then be used to obtain accurate values of G_{Ic} for the onset of crack propagation. On the other hand, examining the load versus time trace shows that, typically within the interval between the crack being stationary and initiating, several load oscillations will have occurred. Hence, defining a critical load for crack initiation from the load versus time trace, is difficult and becomes a matter of debate. Thus, if Equations 6 and 7 are used to deduce values of the fracture energy, G_{Ic}, this difficulty inevitably introduces a high degree of uncertainty and scatter into the values of G_{Ic}.

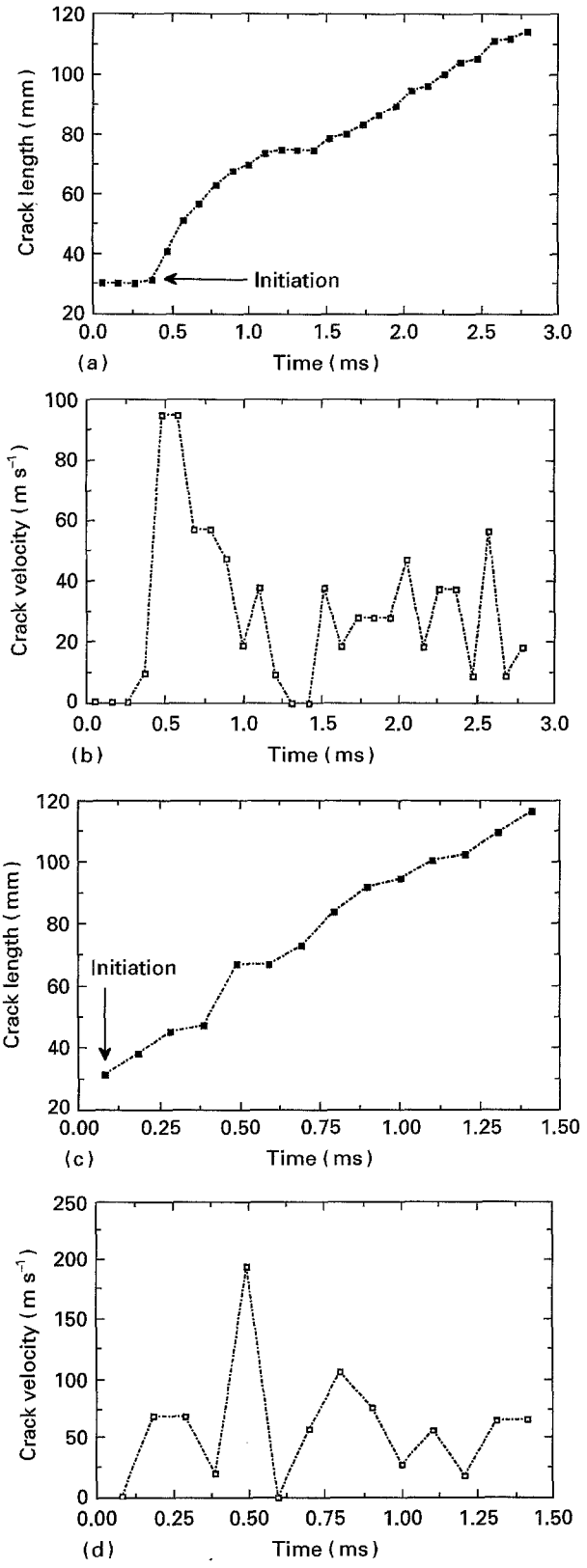

Figure 11 Typical (a, c) crack length and (b, d) crack velocity versus time traces for the epoxy/carbon-fibre composite tests conducted at a ram-displacement rate of (a, b) 5 m s^{-1}, (c, d) 15 m s^{-1}.

4.3. Evaluation of G_{Ic} as a function of crack length

A rising R-curve (i.e. where the value of the fracture energy, G_c increases with the length of propagating delamination) has been previously recorded [3, 4] for the PEEK/unidirectional carbon-fibre composite at relatively slow rates, and this effect was observed in the present studies. At rates of up to $5\,m\,s^{-1}$ the R-curve was still evident, i.e. subsequent initiation values obtained during the "stick–slip" crack growth process did indeed show an increasing trend with crack length. However, at rates above $5\,m\,s^{-1}$, an "R-curve" was not detected.

In the case of the epoxy/unidirectional carbon-fibre composite, no rising R-curve was observed at any of the various test rates which were employed, again in accordance with previous observations [3]. However, at rates of test greater than about $5\,m\,s^{-1}$ there was an indication that a slightly higher value of G_{Ic} occurs immediately after the crack has begun to propagate, the value of G_{Ic} then returning to the initiation value as the crack propagates through the DCB specimen. It is considered that this small peak is associated with the dynamics of such high-rate tests, and will be discussed in Part II [12].

4.4. Effect of test rate on G_{Ic}

For the PEEK/carbon-fibre composite, Fig. 12 shows the values of the interlaminar fracture energy, G_{Ic}, for both crack initiation and arrest (where appropriate) as a function of rate, from rates of specimen displacement from $3.3 \times 10^{-5}\,m\,s^{-1}$ to about $15\,m\,s^{-1}$. (In this, and succeeding graphs, the error bars show the standard deviation determined from the experimental results.) As may be seen, firstly, unstable crack propagation only occurs at rates greater than $8.3 \times 10^{-5}\,m\,s^{-1}$. Secondly, there is no major decrease in the value of G_{Ic} for either initiation, or arrest, with increasing rate. However, a modest reduction in the value of G_{Ic} at crack initiation is apparent at rates in excess of $5\,m\,s^{-1}$. This reduction does not exceed about 20% of the initial static (i.e. low test rate) value of G_{Ic} recorded at crack initiation. This reduction is far less than that reported [7] by some other workers. In this respect it is of interest to note that the reduction in G_{Ic} at crack initiation obtained from the present work would have been far greater if we had employed the unreliable, and inaccurate, values of the measured load at crack initiation to deduce the values of G_{Ic}, as was employed by the previous workers.

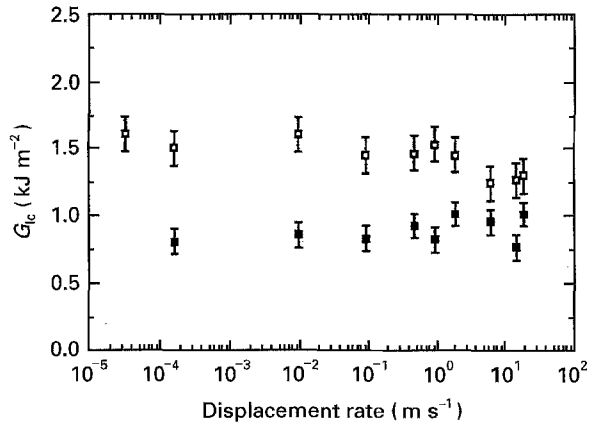

Figure 12 G_{Ic} versus specimen-displacement rate for the PEEK/carbon-fibre composite. (□) crack initiation values, crack arrest values. (■)

In the case of the epoxy/unidirectional carbon-fibre composite, the value of G_{Ic} remains insensitive to the rate of specimen displacement across the entire range of test rates, as shown in Fig. 13.

Finally, it should be noted that we have not taken dynamic effects into account when deducing the values of G_{Ic}; i.e. we have used a static analysis (i.e. Equation 9) to deduce the values of the interlaminar fracture energies. The dynamic effects associated with testing at relatively high rates will be considered in detail in Part II [12]. However, in the context of the present discussion, it should be noted that dynamic corrections to allow for kinetic energy effects are negligible, of course, at the lower rates of test. Furthermore, even at the highest rates of test, such as at $10\,m\,s^{-1}$, such effects are predicted [12] to decrease the values of G_{Ic} given in Figs 12 and 13 by a maximum of about 2% for the PEEK composite and about 8% for the epoxy composite.

5. Results and discussion: adhesive joint specimens

5.1. Load versus time traces

The load traces obtained from testing the adhesive joint specimens show broadly the same trend as those obtained from the PEEK/carbon-fibre composite, namely that stable continuous crack propagation gives way to typical unstable "stick–slip" type propagation as the test rate is increased. The rate at which

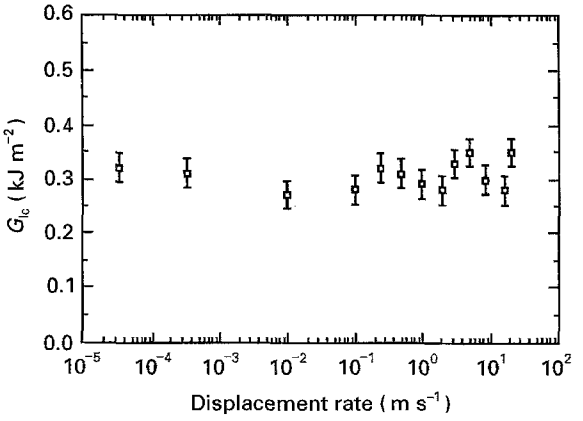

Figure 13 G_{Ic} versus specimen-displacement rate for the epoxy/carbon-fibre composite.

TABLE IV Rates of test for a transition from stable to typical "stick–slip" crack growth for the adhesive joint specimens.

Adhesive	Transition rate ($m\,s^{-1}$)
Epoxy film	3.3×10^{-3}
Epoxy paste	1.67×10^{-2}

the transition from stable to unstable crack propagation occurs depends on the adhesive employed, and the transition rates are shown for the two adhesives in Table IV.

Fig. 14 shows the load versus time signals for the DCB joints bonded using the epoxy-film adhesive. Crack propagation was cohesive, i.e. within the adhesive, at all test rates. Fig. 14a shows a load versus time trace from a test conducted at 3.3×10^{-5} m s^{-1}, i.e. well within the stable regime. The load trace is linear up to the point of crack initiation, after which the crack propagates in a stable manner with a steadily decreasing load being observed. However, Fig. 14b shows an equivalent trace obtained at a rate of 1×10^{-2} m s^{-1}, i.e. above the transition rate, and thus depicts "stick–slip" crack propagation. The process of crack initiation and crack arrest is now repeated along the length of the specimen, and thus gives rise to the type of load versus time trace shown in Fig. 14b. This is clearly similar in nature to that previously described for the PEEK/unidirectional carbon-fibre composite. Fig. 14c shows the load versus time trace resulting from a test at 5×10^{-1} m s^{-1}. This signal demonstrates that although "stick–slip" crack propagation is still evident, the load versus time trace shows an increased dynamic influence, especially at the onset of unstable crack growth. It is at these initiation loads that the fibre composite arms are affected most significantly by flexural wave effects, and this effect may be clearly seen from the high-speed photographic studies. Fig. 14d shows a load versus time recorded at 2 m s^{-1}. It is evident from this trace that the dynamically induced oscillations on the measured values of load are now masking the crack propagation behaviour. The severe oscillations in the load will obviously introduce serious errors into values of G_{Ic} calculated using values of the measured load. Some of the oscillations in the early part of the signal introduce a load fluctuation of up to $\pm$ 40 N, which corresponds to a percentage error in the load values of $\pm$ 25% for crack initiation in this adhesive. Therefore, as for the failure of the fibre composites discussed above, it is easily possible to deduce misleadingly high or low values of G_{Ic}, depending on how the load versus time traces are interpreted. Clearly the use of curve smoothing or data filtering would reduce the amount of load oscillation in the signal, but such techniques have not been employed in the present work for the reasons previously discussed. Similar load versus time signals were also obtained when testing DCB joints bonded using the epoxy-paste adhesive.

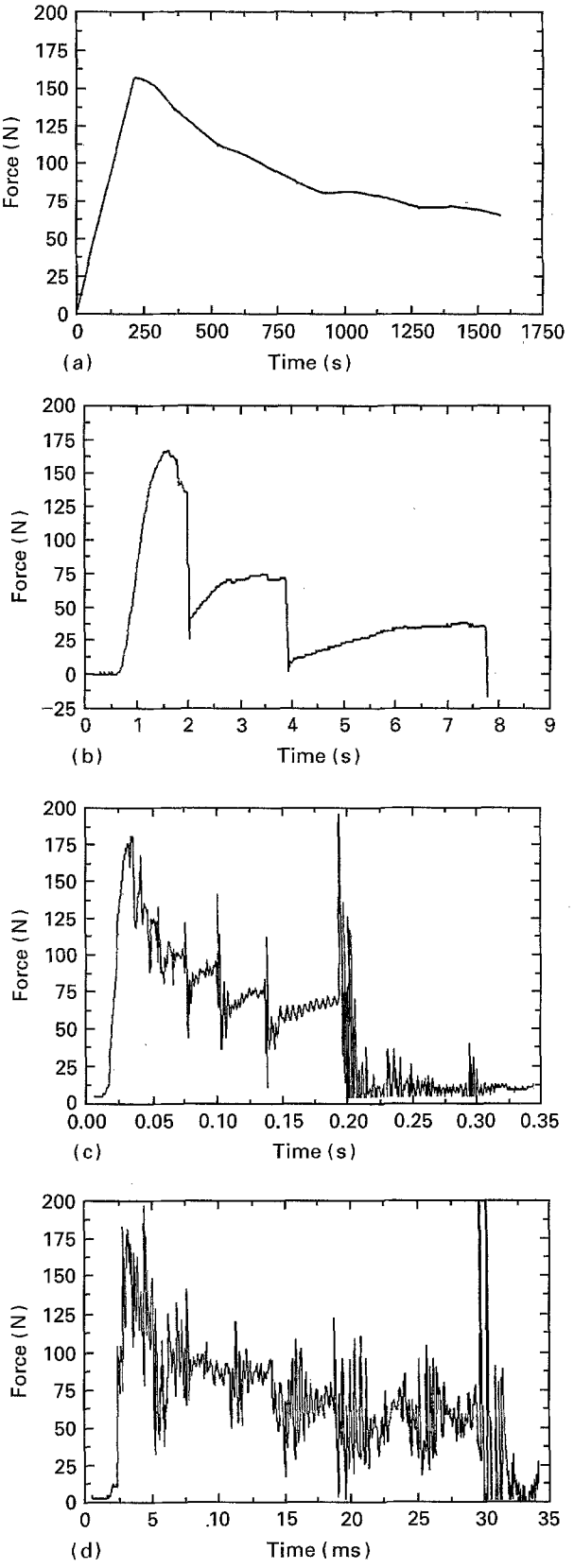

Figure 14 Typical load versus time traces for DCB joints bonded using the epoxy-film adhesive and tested at a ram-displacement rate of (a) 1.67×10^{-5} m s^{-1}, (b) 1×10^{-2} m s^{-1}, (c) 5×10^{-1} m s^{-1}, (d) 2 m s^{-1}.

5.2. Variation of crack length and crack velocity with time

Fig. 15 shows the crack length versus time, and resulting crack velocity versus time, data for joints bonded with the epoxy-film adhesive at various rates. Fig. 15a shows these data at a rate of 1.67×10^{-5} m s^{-1}. At this slow rate, the crack was monitored using the travelling microscope, and it can be seen that the crack grows steadily through the joint. The crack velocity does oscillate somewhat, but tends to decrease with time, i.e. the velocity decreases with an increasing crack length, as would be expected. (Note that the onset of crack propagation is shown in Fig. 15a, 15c and 15e for reference.)

Fig. 15c and d shows the crack length and crack velocity data at a test rate of 2 m s^{-1}. Crack growth is

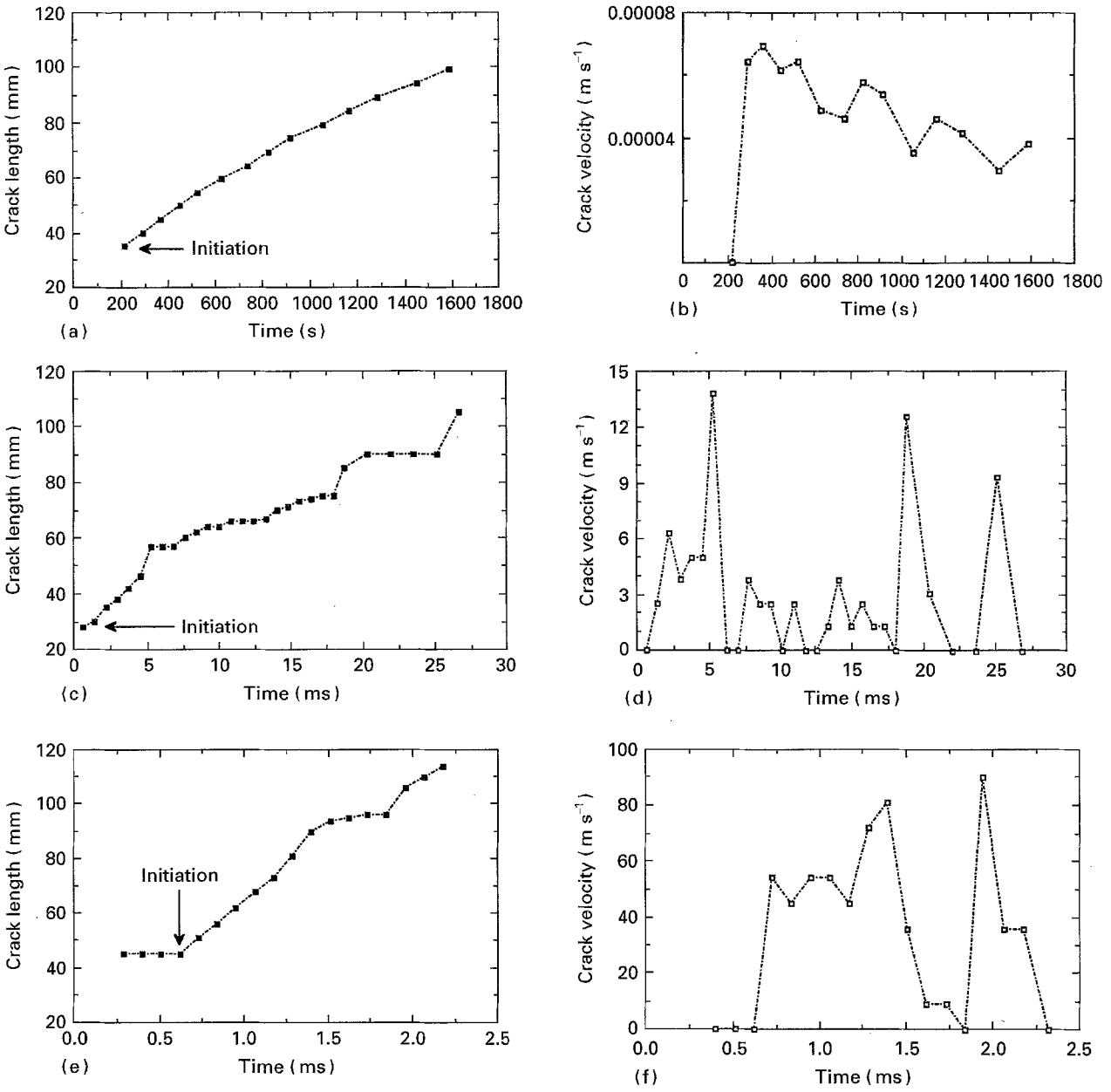

Figure 15 Typical (a, c, e) crack length and (b, d, f) crack velocity versus time traces for DCB joints bonded using the epoxy-film adhesive tested at a ram-displacement rate of (a, b) 1.6×10^{-5} m s^{-1}, (c, d) 2 m s^{-1}, (e, f) 15 m s^{-1}.

now "stick–slip" in nature, as may be seen from Fig. 15c. This is clearly reflected in the resulting crack velocity versus time trace, Fig. 15d. Fig. 15e shows the equivalent crack length, and crack velocity, versus time data at a test rate of 15 m s^{-1}. Again the crack velocity data are transient, now showing a maximum crack speed of almost 90 m s^{-1} followed within half a millisecond by an instance of crack arrest.

5.3. Evaluation of G_{Ic} as a function of crack length

As reported previously [19], the value of the adhesive fracture energy, G_{Ic}, was deduced using the theoretical approach developed in Section 2. Neither of the two adhesives employed in the present work exhibited an *R*-curve, i.e. there was no increase in the value of G_{Ic} with increasing crack length. For each adhesive, the crack remained cohesive in the adhesive layer at all test rates.

When typical "stick–slip" crack propagation was observed, i.e. at rates above the transition rates (see Table IV), it was possible to define the points of crack initiation and crack arrest. At the lower test rates, the arrest value of G_{Ic} were significantly lower than the initiation values. For example, at a rate of 3.3×10^{-3} m s^{-1} the epoxy-film adhesive possessed a G_{Ic} (initiation) value of 2.3 kJ m^{-2} but an arrest value of 1.2 kJ m^{-2}. Also, at a rate of 0.5 m s^{-1}, the epoxy-paste adhesive possessed a G_{Ic} (initiation) value of 4.0 kJ m^{-2}, but an arrest value of only 0.36 kJ m^{-2}. Thus, the adhesive with the higher initiation value of G_{Ic} possessed the lower arrest value.

As the rate of test was increased, the average length that the crack grew on each "stick–slip" cycle decreased; i.e. the stick–slip bands became narrower and more numerous. At the highest test rates, i.e. 10–15 m s^{-1}, the "stick–slip" bands had become sufficiently narrow to give the impression that continuous crack growth had resulted. However, close inspection

of the fracture surfaces clearly revealed that the crack growth mechanism was still "stick–slip" in nature.

5.4. Effect of test rate on G_{Ic}

Values of G_{Ic} for the two adhesives are shown in Figs 16 and 17 as a function of the rate of specimen displacement. These figures show crack initiation values of G_{Ic}; and arrest values where they were obtained, see Table IV. The error bars show the standard deviation determined from the experimental results. Several interesting points are to be seen.

Firstly, the effect of specimen-displacement rate on the performance of the epoxy-film adhesive is shown in Fig. 16. As may be seen, at low rates the initiation value of G_{Ic} is $2.3 \pm 0.15\ kJ\,m^{-2}$. This value is maintained up to a rate of about $10\ m\,s^{-1}$, after which a modest decrease was observed with G_{Ic} decreasing to $1.8 \pm 0.15\ kJ\,m^{-2}$ at $15\ m\,s^{-1}$. The path of joint failure remained cohesive through the adhesive layer at all test rates.

Secondly, as shown in Fig. 17, the epoxy-paste adhesive shows a constant initiation value of G_{Ic} of about $3.8 \pm 0.25\ kJ\,m^{-2}$ up to a specimen-displacement rate of $0.5\ m\,s^{-1}$ after which a steady decrease is recorded with a value at initiation of G_{Ic} of $2.0 \pm 0.25\ kJ\,m^{-2}$ at a rate of about $15\ m\,s^{-1}$. The failure again remained cohesive at all rates, but at the higher rates the fracture surface became significantly more brittle in appearance, as discussed later in Section 5.5.

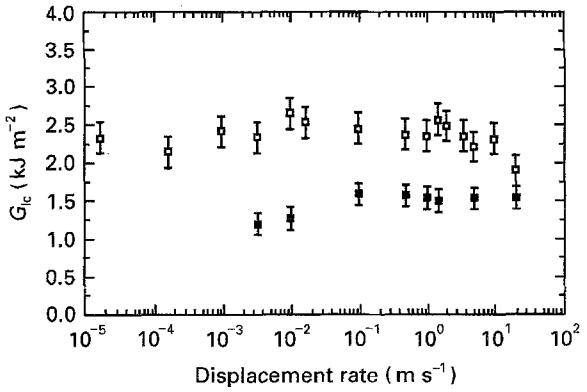

Figure 16 G_{Ic} versus specimen-displacement rate for DCB joints bonded using the epoxy-film adhesive. (□) crack initiation values, (■) crack arrest values.

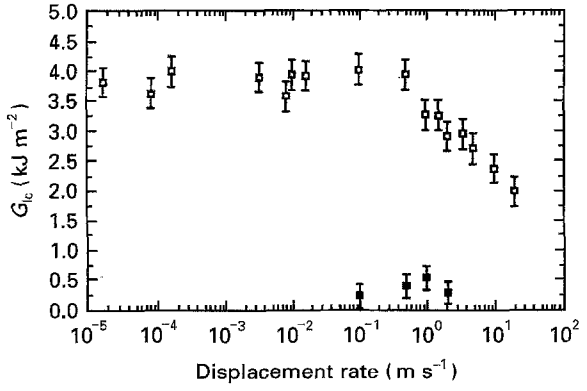

Figure 17 G_{Ic} versus specimen-displacement rate for DCB joints bonded using the epoxy-paste adhesive. (□) crack initiation values, (■) crack arrest values.

Thirdly, considering the aspect of crack arrest, then the arrest values of G_{Ic} are lower than the initiation values, as would be expected, and this is especially the case of the tougher epoxy-paste adhesive. The values of G_{Ic} (arrest) are not significantly dependent upon the rate of test. It should be noted that at rates above about $1\ m\,s^{-1}$ it becomes increasingly difficult to distinguish between points of crack initiation and crack arrest. This is at least partially due to the crack-length distance between the initiation and the arrest points becoming smaller with increasing test rate, as discussed above. Also, at these higher test rates it becomes increasingly difficult for the crack to arrest fully before it is driven on again by the increase in the displacement of the specimen, and thus there is increasing uncertainty as to whether these points represent genuine arrest points. Hence, for the epoxy-paste adhesive, the values of G_{Ic} (arrest) at the highest displacement rates cannot be accurately determined and are not therefore shown in Fig. 17.

Finally, again, it should be noted that we have not taken into account the dynamic effects when deducing the values of G_{Ic}; i.e. we have used a static analysis (i.e. Equation 9) to deduce the values of the adhesive fracture energies, G_{Ic}. The dynamic effects associated with testing at relatively high rates will be considered in detail in Part II [12]. However, in the context of the present discussions, it should be noted that dynamic corrections to allow for kinetic energy effects are negligible, of course, at the lower rates of test. Furthermore, even at the highest rates of test, such as at $10\ m\,s^{-1}$, such effects are predicted [12] to decrease the values of G_{Ic} given in Figs 16 and 17 only by a maximum of about 1.5% for both adhesives.

5.5. Fractographic studies

The reasons for the greater decrease in the adhesive fracture energy, G_{Ic}, for the joints bonded using the epoxy-paste adhesive, i.e. see Fig. 17, may be understood by considering the micromechanisms of failure [20]. Both the epoxy-film and the epoxy-paste adhesives consist of a cross-linked matrix of epoxy polymer which contains a dispersed phase of small rubber particles. The rubber particles having a diameter from submicrometre to 1 or 2 μm.

The presence of the rubber particles greatly increases the toughness of the adhesive and two important toughening mechanisms have been identified for such two-phase materials [20–26]. The first is localized shear yielding, or shear banding, which occurs between the rubber particles at an angle of approximately $\pm 45°$ to the direction of the maximum principal tensile stress [20–26]. Owing to the large number of particles involved, the volume of thermoset matrix material which can undergo plastic yielding is effectively increased compared to the basic single-phase epoxy polymer. Consequently, far more irreversible energy dissipation is involved and the toughness of the material is improved. The second mechanism is the internal cavitation, or interfacial debonding, of the

rubbery particles, which may then enable the subsequent growth of these voids by plastic deformation of the epoxy matrix [24–26]. The importance of this mechanism is that the irreversible hole-growth process of the epoxy matrix also dissipates energy and so contributes to the enhanced fracture toughness. Thus, from the above toughening mechanisms it is evident that the ability of the cross-linked epoxy polymer to undergo plastic yielding is an important requirement, and the rate dependence of the yield and post-yield behaviour of the epoxy, will obviously be important in influencing the rate dependence of the fracture properties of the adhesive.

Now, scanning electron micrographs of the fracture surfaces of the adhesives reveal important differences in the fracture behaviour as the rate of test is increased. At relatively low test-rates the fracture surfaces of both adhesives reveal that plastic deformation of the epoxy has occurred; for example, as may be seen from Fig. 18a. This micrograph clearly shows the development of the plastic hole growth, triggered by the cavitation of the rubbery particles, and the extensive plastic deformation of the epoxy polymer. Further, the more extensive plastic deformation is seen in the case of the tougher epoxy-paste adhesive, as indeed would be expected.

At the highest rates of test, the fracture surface of the epoxy-film adhesive is not greatly different from that recorded at the lower test rates, although somewhat less plastic deformation has apparently occurred. This is in agreement with the observation that the adhesive fracture energy, G_{Ic}, for this adhesive is not greatly affected by the rate of test, see Fig. 16. However, for the epoxy-paste adhesive, the extent of plastic deformation has greatly decreased, as may be seen by comparing Fig. 18a and b. Indeed, in Fig. 18b virtually no plastic hole growth has resulted, and this is reflected in the significantly lower toughness for this adhesive at the high rates of test, see Fig. 17.

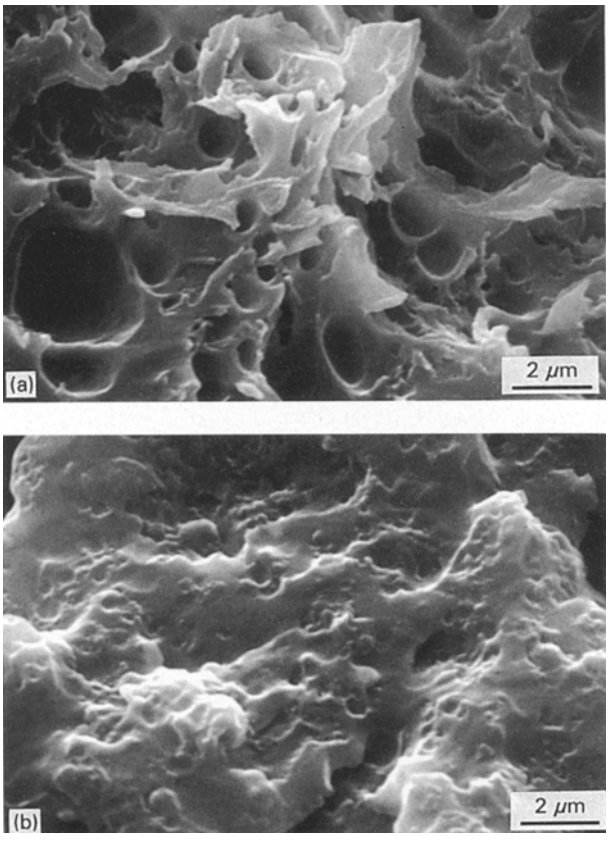

Figure 18 Scanning electron micrographs of the fracture surfaces of the epoxy-paste adhesive tested at a ram-displacement rate of (a) 10^{-5} m s^{-1}, (b) 10 m s^{-1}.

Considering the reasons for these differences in the fracture behaviour of the two adhesives, the hot-curing epoxy-film adhesive has a glass transition temperature, T_g, of about 90 °C, whereas the cold-curing epoxy-paste adhesive has a T_g of about 59 °C. Therefore, the epoxy-paste adhesive is essentially being tested closer to its T_g than the epoxy-film adhesive. This is indeed likely to result in the yield and post-yield properties of the epoxy-paste adhesive being more dependent upon the rate of test. Hence, the extent of localized plastic deformation and the measured fracture energy of the epoxy-paste adhesive will be more dependent upon the rate of test.

6. Conclusion

The present studies have discussed in detail the experimental results from studies designed to measure the mode I failure of fibre composites and adhesively bonded fibre composites under a wide range of rates of test, up to rates of about 15 m s^{-1}.

Firstly, it has been shown that great care must be taken in the experimental aspects when undertaking the tests at high rates of test. For example, the displacement of the ram of the test machine does not necessarily reflect the actual displacement of the specimen, and similarly the loads recorded by the load cell may bear little relationship to the loads actually experienced by the specimen. These, and other dynamic effects, have been identified in the present studies and experimental techniques, and theoretical expressions for the fracture energy, G_{Ic}, for overcoming these problems have been reported. It is considered that, because many of the previous workers apparently have not taken these effects into account, such effects may explain the conflicting results to be found in the literature. Of major importance in this respect is the derivation and use of expressions (e.g. Equation 9) which do not rely upon values of the measured loads in order to deduce values of the fracture energy, G_{Ic}, because the dynamic effects typically cause the measured loads to oscillate violently, and be unreliable and unrepresentative of the loads actually being experienced by the specimen.

Secondly, detailed analysis of the manner in which the crack propagates has shown that, as the rate of test increases, there is an increasing tendency for unstable "slip–stick" crack growth to be observed. The crack velocity versus time data emphasizes the highly transient nature of the crack growth at the higher rates of test, with these maximum transient crack velocities being significantly higher than the velocities measured for the slower test rates.

Thirdly, for the fibre composites, the values of the interlaminar fracture energy, G_{Ic}, deduced from Equation 9 have been plotted against the rate of specimen

displacement. For the PEEK/carbon-fibre composite there is no major decrease in the value of G_{Ic} for either initiation, or arrest, with increasing rate. However, a modest reduction in the value of G_{Ic} at crack initiation is apparent at rates in excess of 5 m s^{-1}. However, this reduction does not exceed 20% of the initial static (i.e. the low-rate) value of G_{Ic} recorded for crack initiation, where the initiation value was 1.6 kJ m^{-2}. This reduction due to increasing the rate of test is far less than that reported [7] by some other workers. To reinforce the comments made above on the dynamic effects associated with high rates of test, it is of interest to note that the reduction in G_{Ic} at crack initiation obtained from the present work would typically have been far greater if we had employed the unreliable and inaccurate values of the measured load at crack initiation in order to determine the values of G_{Ic} via Equations 7 and 8. In the case of the epoxy/carbon-fibre composite, the value of G_{Ic} remained insensitive to rate across the entire test-rate range, the value being about 0.3 kJ m^{-2}.

Turning now to the adhesively bonded fibre composite joints, the effect of specimen-displacement rate on the value of G_{Ic} of the epoxy-film adhesive reveals that, at low displacement rates, the initiation value of G_{Ic} is about 2.3 kJ m^{-2}. This value is maintained up to a rate of about 10 m s^{-1}, after which a modest decrease is observed, with G_{Ic} decreasing to 1.8 kJ m^{-2} at 15 m s^{-1}. The tougher epoxy-paste adhesive showed a constant value of G_{Ic} of about 3.8 kJ m^{-2} up to a rate of 0.5 m s^{-1}, after which a steady decrease was recorded, with a value of G_{Ic} at initiation of 2.0 kJ m^{-2} at a test rate of 15 m s^{-1}. Thus, the tougher epoxy-paste adhesive shows the greater rate dependence. The failure for the adhesive joints employing either the epoxy-film or the epoxy-paste adhesive is cohesive through the adhesive at all rates.

Part II will discuss, and analyse in detail, the dynamic effects which are invariably associated with high-rate tests, and will show how these effects influence the observed behaviour of the test specimens. Part III will report the results from mode II and mixed-mode I/II tests on the fibre composite materials.

Acknowledgements

The authors thank the Engineering Physical Sciences Research Council for financial support and the Polymer Engineering Group, ICI plc, and Ciba Composites, for general support. They also thank Dr P. Cawley, Imperial College, Department of Mechanical Engineering, and his research group for assistance with the ultrasonic measurements.

References

1. J. M. WHITNEY, C. E. BROWNING and W. HOOGSTEDEN, *J. Reinf. Plastics Compos.* **1** (1982) 297.
2. P. E. KEARY, L. B. ILCEWICZ, C. SHAAR and J. TROSTLE, *J. Compos. Mater.* **19** (1985) 154.
3. S. HASHEMI, A. J. KINLOCH and J. G. WILLIAMS, *Proc. R. Soc.* **A427** (1990) 173.
4. *Idem, J. Compos. Mater.* **24** (1990) 918.
5. A. J. KINLOCH, Y. WANG, J. G. WILLIAMS and P. YAYLA, *Compos. Sci. Technol.* **47** (1993) 225.
6. A. J. KINLOCH, "Adhesion and adhesives: science and technology", (Chapman and Hall, London, 1987).
7. A. J. SMILEY and R. B. PIPES, *J. Compos. Mater.* **21** (1987) 670.
8. PH. BEGUELIN, M. BARBEZAT and H. H. KAUSCH, *J. Phys. III Fr.* **1** (1991) 1867.
9. A. A. ALIYU and I. M. DANIEL, ASTM STP **876** (American Society for Testing and Materials, Philadelphia PA, 1985) p. 336.
10. G. YANIV and I. M. DANIEL, ASTM STP **972** (American Society for Testing and Materials, Philadelphia, PA, 1988) p. 241.
11. H. MAIKUMA, J. W. GILLESPIE and D. J. WILKINS, *J. Compos. Mater.* **24** (1990) 124.
12. B. R. K. BLACKMAN, A. J. KINLOCH, Y. WANG and J. G. WILLIAMS, *J. Mater. Sci.* to be published.
13. B. R. K. BLACKMAN, J. P. DEAR, A. J. KINLOCH, H. MacGILLIURAY, Y. WANG, J. G. WILLIAMS and P. YAYLA, *ibid.* to be published.
14. S. HASHEMI, A. J. KINLOCH and J. G. WILLIAMS, *Compos. Sci. Technol.* **37** (1990) 429.
15. H. SETIAWAN, PhD thesis, University of London (1995).
16. D. N. ALLEYNE and P. CAWLEY, *NDT & E Int.* **25** (1992) 11.
17. H. KOLSKY, "Stress waves in solids" (Constable, Dover Publications, New York, USA, 1963).
18. J. HARDING and L. M. WELSH, *J. Mater. Sci.* **18** (1983) 1810.
19. B. R. K. BLACKMAN, J. P. DEAR, A. J. KINLOCH and S. OSIYEMI, *J. Mater. Sci. Lett.* **10** (1991) 253.
20. A. J. KINLOCH, in "Rubber-toughened plastics", edited by C. K. Riew, Advances in Chemistry Series **222** (American Chemical Society, Washington, DC, 1989) p.67.
21. A. J. KINLOCH, S. J. SHAW and D. L. HUNSTON, *Polymer* **24** (1983) 1355.
22. A. F. YEE and R. A. PEARSON, *J. Mater. Sci.* **21** (1986) 2462.
23. R. A. PEARSON and A. E. YEE, *ibid.* **21** (1986) 2475.
24. Y. HUANG and A. J. KINLOCH, *ibid.* **27** (1992) 2753.
25. *Idem, ibid.* **27** (1992) 2763.
26. *Idem, Polymer* **33** (1992) 1330.

Received 25 May
and accepted 7 June 1995